

The Effect of ENSO Events on the Tropical Pacific Mean Climate: Insights from an Analytical Model

JIN LIANG

*Institute for Climate and Global Change Research, School of Atmospheric Sciences, Nanjing University, Nanjing, China,
and Cooperative Institute for Research in Environmental Sciences, University of Colorado and NOAA/Earth System
Research Laboratory/Physical Science Division, Boulder, Colorado*

XIU-QUN YANG

Institute for Climate and Global Change Research, School of Atmospheric Sciences, Nanjing University, Nanjing, China

DE-ZHENG SUN

*Cooperative Institute for Research in Environmental Sciences, University of Colorado and NOAA/Earth System
Research Laboratory/Physical Science Division, Boulder, Colorado*

(Manuscript received 31 August 2011, in final form 19 April 2012)

ABSTRACT

To better understand the causes of climate change in the tropical Pacific on decadal and longer time scales, the authors delineate the rectification effect of ENSO events into the mean state by contrasting the time-mean state of a low-order model for the Pacific with its equilibrium state. The model encapsulates the essential physics of the ENSO system, but remains simple enough to allow for the obtaining of its equilibrium state. The model has an oscillatory regime that resembles the observations. In this oscillatory regime, the time-mean SST in the eastern equatorial Pacific is found to be significantly different from the corresponding equilibrium SST, with the former being warmer than the latter. The difference is found to be proportional to the amplitude of ENSO. In addition, the zonal SST contrast of the time-mean state is found to be less sensitive to increases in external forcing than that of the equilibrium state, due to warming effect of ENSO events on the eastern Pacific. It is further shown that this rectification effect of ENSO events results from the nonlinear advection term in the heat budget equation. The study elucidates the role of ENSO events in shaping the tropical mean climate state and suggests that decadal warming in the recent decades in the eastern tropical Pacific may be more a consequence than a cause of the elevated ENSO activity during the same period. The results also provide a simple explanation for why it is difficult to detect an anthropogenically forced trend in the zonal SST contrast in the observations.

1. Introduction

The importance of the tropical Pacific sea surface temperature (SST) in predicting climate variability over North American and the world at larger has been vividly demonstrated in our rich experience with ENSO (Philander 1990). The apparent regimelike shift in the tropical Pacific SST from about 1976 has underscored

another fact about tropical Pacific SST: it also varies on decadal time scales (Wang and Ropelewski 1995; Zhang et al. 1997; Fedorov and Philander 2000). As the society increasingly needs a climate outlook beyond the time scale of ENSO, understanding the mechanisms that give rise to the decadal variability in the background state of ENSO (or the time-mean state relative to the time scale of ENSO) has become a forefront issue facing climate research community (Meehl et al. 2010).

This regime shift shown in Fig. 1a is accompanied with the change in the level of ENSO variability—the variance of the interannual variability of the tropical Pacific SST (Fig. 1b). The level of ENSO activity during the epoch with a warmer time-mean SST in the eastern

Corresponding author address: Dr. De-Zheng Sun, Cooperative Institute for Research in Environmental Sciences, University of Colorado and NOAA/Earth System Research Laboratory/Physical Science Division, Boulder, CO 80304.
E-mail: dezhen.sun@noaa.gov

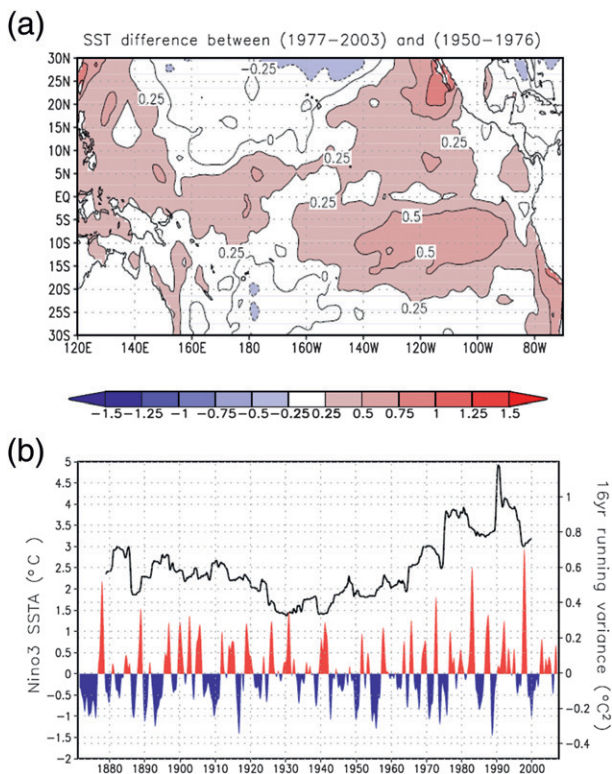


FIG. 1. (a) SST differences between two epochs: 1977–2003 and 1950–76. (b) Niño-3 SST time series. Niño-3 SST (anomalies) (in color). The black solid line is the variance of Niño-3 SST anomalies obtained by sliding a moving window of a width of 16 yr. Note that the epoch 1977–2003 has higher level of ENSO activity than the previous period 1950–76. (SST data used are from the Hadley Center for Climate Prediction and Research) (Rayner et al. 1996).

tropical Pacific is anomalously higher than the previous epoch with a colder time-mean SST in the eastern tropical Pacific. Is the change in the level of ENSO activity caused by the change in the time-mean state, or is the change in the time-mean state a consequence of the change in the level of ENSO activity? A numbers of studies have examined the impact of a warming in the mean state of the tropical Pacific on the level of ENSO activity (Deng et al. 2010; Fedorov and Philander 2000, 2001; An and Jin 2001; Wang and An 2001, among others). These studies employ the traditional linear instability analysis of the mean state and deduce the impact of changes in the mean state on the growth rate of the ENSO modes. These studies have nicely illuminated a consistency between the changes in the level of ENSO activity and the corresponding changes in the time-mean state, within the mathematical framework of linear instability analysis. However, these studies do not address the cause of the warming in the time-mean state, in particular the question of whether an increase in the level of ENSO activity can induce a warming in the time-mean

state. We here employ a different methodology and explore the possibility that the decadal warming over the eastern Pacific is due to the rectification effect of elevated ENSO events into the mean state (i.e., the time-mean effect of ENSO events).

The possibility that ENSO may have an important time-mean effect on the tropical Pacific climatology has been highlighted by preliminary studies of the role of ENSO in the heat balance of the tropical Pacific. In a numerical experiment with a coupled model, Sun and Zhang (2006) found that the response in the upper ocean temperature to an increase in the tropical heating is very different between the case with ENSO and the case without ENSO. The presence of ENSO can increase considerably the response in the subsurface temperature, and shift the maximum surface level response from the western Pacific warm pool to a broad region in the central and eastern Pacific. Sun and Zhang (2006) further noted that this time-mean effect of ENSO is linked to an asymmetric response to an increase in the tropical heating between the two phases of ENSO.

The surface manifestation of the asymmetry between El Niño and La Niña events—the strongest El Niño event, measured by the Niño-3 SST anomaly, is stronger than the strongest La Niña event—has long been noted (Zebiak and Cane 1987; Burgers and Stephenson 1999). It has also been suggested by recent studies that decadal variability may result from a “residual” effect of ENSO on the background state due to the asymmetry between El Niño and La Niña events (Rodgers et al. 2004; Sun and Yu 2009). Rodgers et al. (2004) found in a long simulation by a coupled GCM that changes in the mean state between decades with high ENSO activity and decades with low ENSO activity resemble the residual of the two phases of ENSO in the model. They therefore suggest that the asymmetry could be a mechanism for decadal changes in the tropical Pacific SST. Noting a 15-yr cycle in the level of ENSO activity in an extended SST dataset consisting of historical and paleoclimate data, and a change in the asymmetry of ENSO with this decadal cycle, Sun and Yu (2009) have argued that the residual effect from the ENSO asymmetry may provide an explanation for the decadal cycle they have noted in the level of ENSO activity.

Specific mechanisms have also been proposed to explain the asymmetry between the two phases of ENSO. Jin et al. (2003) and An and Jin (2004) suggested that the asymmetry is due to the nonlinear term in the heat budget equation for the surface ocean. Schopf and Burgman (2006) showed that the skewness of the SST distribution could be due to a kinematic effect of oscillating a nonlinear temperature profile. While the relative contributions to the asymmetry between the two phases of ENSO

from these two mechanisms need to be further studied, these studies suggest that the nonlinear aspects of ENSO are important, and a climate regime that has a higher level of ENSO activity may result in a different time-mean climate because the effects of stronger El Niño events may not be balanced by a corresponding change in the strength of the La Niña events.

Although the aforementioned studies are suggestive about a significant time-mean effect of ENSO on the climatology, this effect remains to be delineated clearly. We may divide the observations and model simulations of ENSO into epochs with different levels of ENSO activity and then try to discern the time-mean effect of ENSO by contrasting the mean states of these epochs as done in Rodgers et al. (2004), but this approach only confirms a correspondence between a change in the level of ENSO activity and a change in the mean state. The asymmetry between the two phases of ENSO only suggests a nonzero residual effect of ENSO, to the extent that a finite threshold value is used to define El Niño and La Niña events. But the asymmetry alone is not a sufficient condition for a significant time-mean (or rectification) effect of ENSO because such a residual effect will depend quantitatively on how one defines El Niño and La Niña events.

Ideally, we want to contrast the equilibrium state of the coupled tropical ocean–atmosphere system in which ENSO as an instability has not manifested with the actual realized climatology in which ENSO has manifested. The difficulty for doing so is that if the equilibrium state of the coupled tropical ocean and atmosphere is unstable, it is by definition not observed. The same difficulty exists for complex GCMs whose state evolutions have to be obtained by numerical integration of a set of equations, which also misses the unstable equilibrium state. In this paper, we present a low-order analytical system for the coupled tropical ocean–atmosphere system to explore the effects of ENSO on the time-mean state. The model encapsulates the essential physics of ENSO and has been shown to capture the major characteristics of ENSO (Sun 1997; Timmermann and Jin 2002). The realized time-dependent state in the model can be calculated numerically; the equilibrium state can be obtained analytically. Thereby, we can delineate the role of ENSO events in the climatology (i.e., the time-mean state) by comparing the two states. With this methodology, we will also be able to address another question, which is whether ENSO plays a role in determining the sensitivity of the climatology of the tropical Pacific to a change in external forcing. The methodology we employ is analogous to that used by Manabe and his collaborators in their attempt to establish the effect of moist convection on the mean climate: they calculated the radiative equilibrium of their

model atmosphere and compared it with the radiative-convective equilibrium of their model atmosphere (Manabe and Möller 1961; Manabe and Strickler 1964; Manabe and Wetherald 1967).

This paper is organized as follows. We first briefly describe the model in section 2. We then present the main results concerning the differences between the time-mean state and the equilibrium state in section 3. In section 4 we will discuss the asymmetry of the oscillation in the model in connection with the differences between the time-mean state and the equilibrium state. The nonlinearity responsible for the rectification effect of ENSO events is isolated in section 5. A summary and discussion are provided in section 6.

2. The model

We use the model of Sun (1997, 2000). It is an extension of the model of Sun and Liu (1996) adding the thermocline dynamics in the manner given by Jin (1996). The heat budget of the ocean surface layer can be written as

$$\frac{dT_1}{dt} = c(T_e - T_1) + sq(T_2 - T_1), \quad (1)$$

$$\frac{dT_2}{dt} = c(T_e - T_2) + q(T_{\text{sub}} - T_2), \quad \text{and} \quad (2)$$

$$s = \frac{U}{L_x} \frac{W}{H_1}, \quad (3)$$

where T_1 and T_2 represent the western and eastern equatorial Pacific surface temperature, respectively; T_e is the radiative-convective equilibrium temperature; $1/c$ is a typical thermal damping time scale; T_{sub} is the subsurface ocean temperature; $q = W/H_1$, where W is the upwelling velocity in the equatorial eastern Pacific and H_1 is the depth of the mixed layer; and zonal mass flux is assumed to be a fraction of the total upwelling and this fraction can be measured by s . Also, L_x in Eq. (3) represents the half zonal width of the basin, and U represents the zonal velocity. The value of q is given by

$$q = \frac{\alpha}{a}(T_1 - T_2), \quad (4)$$

where α measures the sensitivity of wind stress to changes in the SST gradients, and a defines the adjustment time scale of the ocean currents to surface winds. The subsurface temperature T_{sub} depends strongly on the eastern Pacific thermocline depth and can be parameterized as

$$T_{\text{sub}} = \Phi(-H_1 + h'_2) \quad \text{and} \quad (5)$$

$$\Phi(z) = T_e - \frac{T_e - T_b}{2} \left[1 - \tanh\left(\frac{z + z_0}{H^*}\right) \right]. \quad (6)$$

Here h'_1 and h'_2 are the western and eastern equatorial thermocline anomalies; z_0 is the depth at which W takes its characteristic value. Also, H^* measures the sharpness of the thermocline; T_b may be regarded as the temperature of the deep ocean. Following Jin (1996), h'_1 and h'_2 are governed by the following two equations:

$$h'_2 - h'_1 = -\frac{H_1}{H_2} H \frac{\alpha}{b^2} (T_1 - T_2) \quad \text{and} \quad (7)$$

$$\frac{1}{r} \frac{dh'_1}{dt} = -h'_1 + \frac{H_1}{2H_2} H \frac{\alpha}{b^2} (T_1 - T_2). \quad (8)$$

A balance between zonal pressure gradients and zonal wind stress is shown in Eq. (7). Note that $H_2 = H - H_1$, with H being the zonal mean depth of the upper ocean at rest. Also, $b = c_k/L_x$, where c_k is the speed of the first baroclinic Kelvin wave. A slow adjustment process of the thermocline depth to its equilibrium value determined by the surface wind stress and mass conservation is adopted in Eq. (8). Parameter r in Eq. (8) measures the time scale for this slow adjustment process. As shown by Sun (1997) and Timmermann and Jin (2002), the model simulates the major characteristics of observed ENSO. Readers are referred to these two studies for temporal characteristics of the oscillation (i.e., time series of T_1 , T_2 , h'_1 , and h'_2) simulated by the model. The focus of the present presentation is on the differences between the time-mean state and the equilibrium state of the model. We will discuss, however, the asymmetry of the oscillation in the model in relation to the differences between the time-mean state and the equilibrium state of the model.

3. The differences between the time-mean state and the equilibrium state

The time-mean state and the equilibrium state of the western equatorial Pacific SST (T_1) and the eastern equatorial Pacific SST (T_2) as a function of T_e are shown in Fig. 2a herein. The equilibrium state of the system has already been shown in Fig. 2 in Sun (1997); here we add the plot of time-mean state to contrast its difference from the equilibrium state. The parameters used here are the same as in Sun (1997). A standard Runge–Kutta method of fourth order is used to integrate the model equations and thereby obtain the time-mean state. The equilibrium state is obtained by setting the time derivatives on the left-hand side of Eqs. (1), (2), (7), and (8) to zero, and then reducing Eqs. (1)–(8) to a single nonlinear algebraic equation.

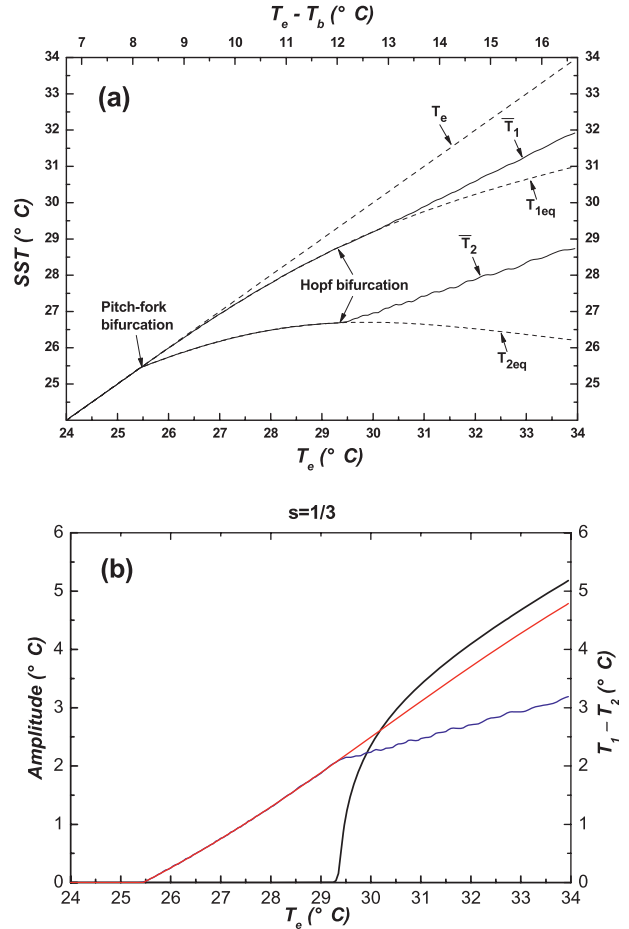


FIG. 2. (a) Equatorial Pacific SST as a function of T_e ; T_1 and T_2 are, respectively, for the western and eastern Pacific SST. Solid lines are for the time-mean state, and the dashed lines are for the equilibrium state. (b) Amplitude of oscillation for T_2 as a function of T_e . The amplitude is defined here as the half-value of the difference between the maximum and minimum value of T_2 . Also shown are the zonal SST contrast as measured by the difference between T_1 and T_2 for the equilibrium state (red) and the time-mean state (blue). Note that the rate of increase in the zonal contrast in the time-mean state with T_e is less than half of the corresponding rate of increase in the equilibrium state (0.25 vs 0.56). The parameter values used in this figure are the same as in Sun (1997, 2000) ($s = 1/3$, $T_b = 17.3^\circ\text{C}$, $1/c = 150$ days, $1/r = 300$ days, $H^* = 65$ m, $H_1 = 50$ m, $H_2 = 150$ m, $z_0 = 75$ m, $\alpha/a = 3.0 \times 10^{-8} \text{ K}^{-1} \text{ s}^{-1}$, $\{[H_1(H_1 + H_2)]/2H_2\}(\alpha/b^2) = 11.5 \text{ m K}^{-1}$).

As described by Sun (1997), Fig. 2a shows that when the radiative forcing T_e achieves 25.5°C , a pitchfork bifurcation (Strogatz 2001) of the system takes place and the coupled system starts to have SST gradients, winds, and currents. Further increasing T_e to 29.3°C , the system experiences a Hopf bifurcation (Strogatz 2001) and begins to enter an oscillatory state. The amplitude of the oscillation increases with further increase in T_e (Fig. 2b). The time-mean value and the equilibrium value of either

T_1 or T_2 are the same before the occurrence of Hopf bifurcation, validating the accuracy of the numerical methods used to obtain the time-mean state. After the system enters the oscillatory regime, the two states are significantly different. The time-mean values of T_2 (or T_1) in the presence of ENSO are observed to be larger than the corresponding equilibrium value under a given radiative forcing, and this discrepancy between the two values becomes even larger as we further increase the value of T_e to increase the amplitude of ENSO.

The difference in T_2 between the two states is much more profound than the difference in T_1 . The two T_2 actually go in opposite directions as T_e increases in the presence of ENSO oscillation. The equilibrium T_2 decreases as T_e increases, a result that is reminiscent of that from Clement et al. (1996) [see also Cane et al. (1997)]. However, the time-mean value of T_2 increases with the increase of T_e . Note that in the present model, the background subsurface temperature is allowed to change in response to changes in T_e according to (5) and (6) while that in the Zebiak–Cane model (Zebiak and Cane 1987)—the model used by Clement et al. (1996)—is fixed. As discussed by Sun (2003), who employs an ocean model [the model of Gent and Cane (1989)] that has a heat budget for the subsurface ocean, the present approach implicitly takes into account the rectification effect of ENSO events on the reference subsurface temperature profile in a way that is consistent with the results from the more complicated ocean model used in Sun (2003).

For a given T_e , the time mean value of T_2 is much warmer than its equilibrium value. Correspondingly, the zonal SST contrast in the time-mean state is much reduced from that in the equilibrium state. Given that the stability of the system is determined by the zonal SST contrast (Jin 1997; Sun 1997), the time-mean state is more stable than the equilibrium state. So the reason behind the warming effect of ENSO events on the eastern Pacific is that ENSO events tend to neutralize the equilibrium state. [To bring this explanation to a general framework for what instability generally does to its mean state, we recall that tropical deep convection collectively warms the upper troposphere and maintains a moist adiabatic lapse rate (Xu and Emanuel 1989). In other words, what ENSO events in the coupled ocean–atmosphere system do to the time-mean zonal SST contrast is analogous to what convective events in the tropical atmosphere do to the time-mean lapse rate].

Because the time-mean value of T_2 increases as T_e increases while the equilibrium T_2 actually decreases, the time-mean zonal SST contrast in the presence of ENSO increases at a much smaller rate than the equilibrium zonal SST contrast. The former is about $0.25^\circ\text{C} (1^\circ\text{C})^{-1}$ increase in T_e while the latter is $0.58^\circ\text{C} (1^\circ\text{C})^{-1}$

increase in T_e . This reduced sensitivity may explain the difficulty in detecting the anthropogenically forced increase in the zonal SST contrast in the observations (Vecchi et al. 2008): the data we have are not yet good enough to detect this small change. We will return to this point in the summary section.

Differences between the time-mean subsurface ocean temperature T_{sub} and the equilibrium T_{sub} in the presence of ENSO oscillation are similar to those between the time-mean and the equilibrium T_2 , but are more pronounced, consistent with the observations (Fig. 3a). The time-mean value of T_{sub} increases as T_e increases in the presence of ENSO, in contrast with its equilibrium solution, which decreases. The relationship between T_{sub} and T_e shows even stronger nonlinearity than that between T_2 and T_e , indicating the importance of subsurface dynamics. As expected, the time-mean upwelling is less strong than that in the equilibrium state [recall Eq. (3)] (Fig. 3b). In the presence of ENSO, the depth of the thermocline in the east is deeper in the time-mean state than in the equilibrium state (Fig. 3c). The reverse is true for the thermocline in the west (Fig. 3d). As the amplitude of ENSO increases, the depth of the thermocline in the time-mean state in the east Pacific becomes increasingly deeper than that in the equilibrium state, underscoring the impact of ENSO on the depth of the thermocline.

Using the same model, Timmermann and Jin (2002) showed that the temporal characteristics of the oscillation can be sensitive to the choice of s . For example, they found that a periodic solution described by Sun (1997) can become chaotic when the strength of zonal advection relative to the strength of the upwelling (the parameter s) is reduced while keeping the value of T_e fixed. We investigate whether the findings concerning the effect of ENSO on the tropical Pacific mean state depend on the details of ENSO characteristics by varying the value of s .

The case shown in Fig. 2 has the value of s set to $1/3$. Figure 4 shows two more cases with s set respectively to 0 (Figs. 4a,b) and 0.096 (Figs. 4c,d). Figures 4a,b and Figs. 4c,d correspond to the two panels in Fig. 2. When we reduce the strength of zonal advection to be neglected ($s = 0$), the two states of eastern equatorial Pacific SST T_2 again diverge after the Hopf bifurcation takes place and brings in the existence of ENSO. Note that Hopf bifurcation occurs at a much smaller value of T_e ($T_e = 26.8^\circ\text{C}$), indicating a stabilizing role from the existence of zonal advection. Unlike the case with $s = 1/3$, the difference in T_2 between the two states in the case with $s = 0$ does not increase monotonically as T_e increases. It comes to its maximum value at $T_e = 28^\circ\text{C}$, when the amplitude of ENSO reaches its maximum, and then decreases rapidly as the amplitude of ENSO decreases

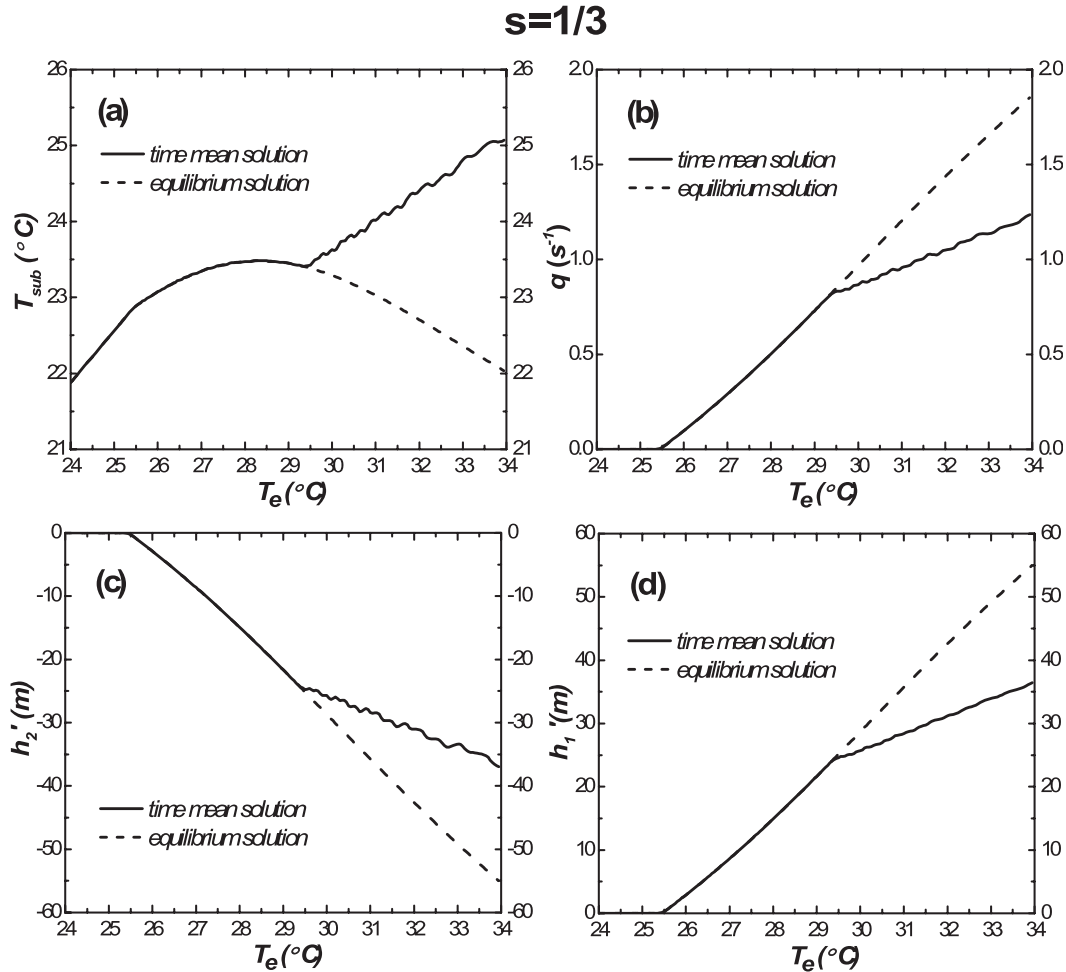


FIG. 3. As in Fig. 2a, but for the (a) subsurface temperature, (b) upwelling, (c) thermocline depth of the eastern equatorial Pacific (anomaly), and (d) depth of the thermocline in the western equatorial Pacific (anomaly). Note that a negative anomaly in h_2' means a reduction in the thermocline depth. The positive difference between the time-mean solution of h_2' and the equilibrium h_2' in the presence of ENSO implies a deepening of h_2' in the eastern Pacific due to the presence of ENSO.

(Fig. 4b). The two states merge into a single one again at $T_e = 28.3^\circ\text{C}$ when the oscillation disappears completely. This confirms that the differences between the two states are proportional to the amplitude of ENSO. Figure 4a shows clearly again that in the presence of ENSO, the time-mean T_2 is warmer than the equilibrium T_2 . (i.e., the time mean state of the equatorial eastern Pacific in the presence of ENSO is warmer than the equilibrium state in which ENSO is mathematically prevented from occurring) Figures 4c and 4d show the case with $s = 0.096$, a value close to the one used by Timmermann and Jin (2002). Again, the results confirm the effect of ENSO on the mean state of the tropical Pacific: In the presence of ENSO, the two states are different with the time-mean T_2 warmer than the equilibrium T_2 . Also, note that the regime of oscillation

becomes wider as the value of s increases, presumably because zonal advection plays a stabilizing role as zonal advection is a cooling mechanism for the western Pacific. It has been shown by earlier studies that zonal advection is significant in observations and may play an important role in ENSO dynamics (Picaut et al. 1997; Fedorov and Philander 2001).

4. The asymmetry of the oscillation in the model

The oscillation immediately after the Hopf bifurcation is regular. As the value of T_e further increases, the oscillation can become irregular. Figures 5a and 5b present the time series of T_2 at $T_e = 28^\circ\text{C}$ and $T_e = 31^\circ\text{C}$ for the case with $s = 0.096$. The equilibrium and time-mean values of T_2 are also added to the figure as horizontal lines to

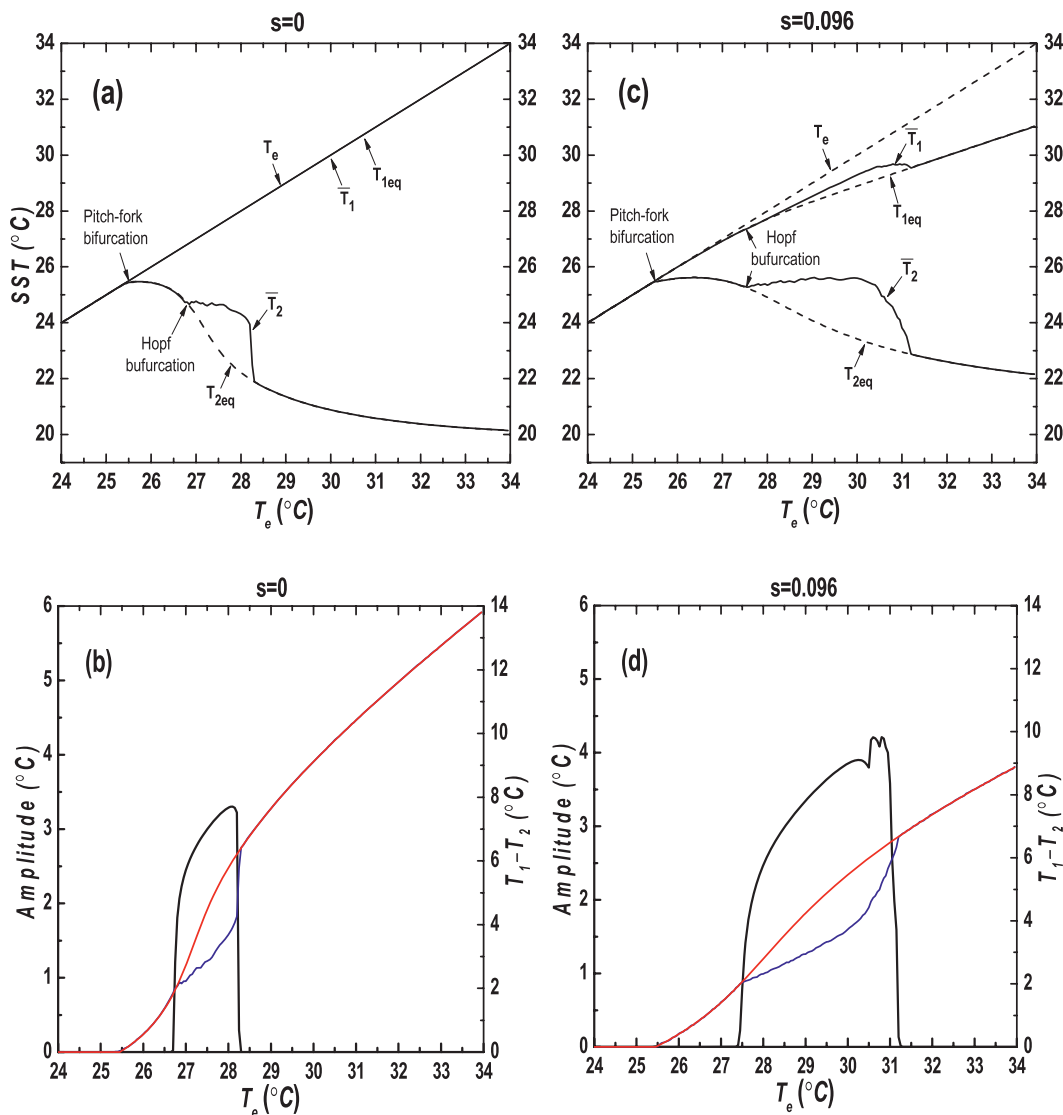


FIG. 4. As in Fig. 2, but for (a),(b) $s = 0$ and (c),(d) $s = 0.096$.

highlight the asymmetry of the oscillation and its possible connections with the differences between the equilibrium value and the time mean value. The figure shows that the system has a regular oscillation at $T_e = 28^\circ\text{C}$ (Fig. 5a) and an irregular oscillation at $T_e = 31^\circ\text{C}$ (Fig. 5b).

In either the regime with regular oscillation or the regime with irregular oscillation, oscillations are asymmetric with respect to the time-mean value: the warm anomaly relative to the long-term time mean is not a mirror image of the cold anomaly relative to the same long-term time mean. In the regime with regular oscillation, the main asymmetry is in the duration of the warm and cold events. The warm anomaly (relative to the time mean) lasts longer than the cold events. The

asymmetry of the oscillation is more profound measured by the departure from the equilibrium state. It is interesting to see that the system lingers on the warmer side of the system longer than its colder side. Note that the cold side has a stronger zonal SST contrast and therefore a stronger current [recall Eq. (4)].

As the system enters the irregular regime, the main asymmetry is in the magnitude of the warm and cold events (Fig. 5b). In the irregular regime, the system has weak and strong warm events. The stronger warm events now have a larger amplitude than the cold events. The cold events also vary in magnitude, but the variation is less than in the magnitude of the warm events. The asymmetry in the irregular regime has a close resemblance to the observed ENSO asymmetry (Burgers and Stephenson 1999).

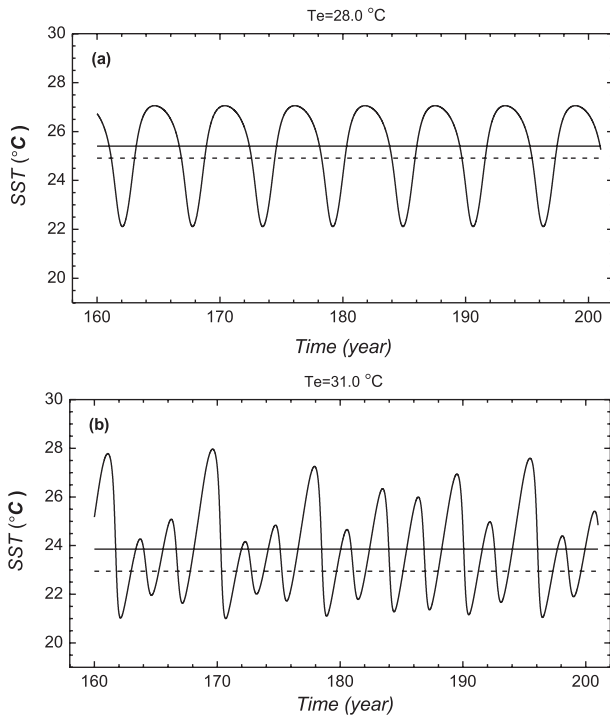


FIG. 5. Time series of T_2 when (a) $T_e = 28^\circ\text{C}$ and (b) $T_e = 31^\circ\text{C}$. The time series are taken from the case with $s = 0.096$ (Figs. 4c,d). The two horizontal lines in the figure indicate respectively the time-mean value of T_2 (solid) and its equilibrium value (dashed).

Relative to the equilibrium state, the asymmetry between the warm events and the cold events in the irregular case is more profound. The equilibrium state almost sets the limit of how cold the system can get (Fig. 5b). When the system does get to the colder side, it quickly escapes to the warmer side. This asymmetry of the oscillation relative to the equilibrium state is even more profound measured in the subsurface. Figure 6a shows the time series of h_1' that corresponds to Fig. 5b. The dashed line again denotes the corresponding equilibrium value. Measured by h_1' , the system rarely exceeds the limit set by the equilibrium state. As found in Zhang et al. (2009), ENSO in the observations also has a stronger asymmetry in its subsurface signature than the surface signature. To highlight this impression, we further present in Fig. 6b the trajectory of the system projected to the plan of T_2 and h_1' with the equilibrium state and the time mean state also marked on the figure. It shows more vividly the one-sided preference of the system relative to its equilibrium state. It suggests strongly that the rectification effect of ENSO into the time-mean state stems fundamentally from the asymmetry of the dynamics of the system relative to its equilibrium state.

The asymmetry of the dynamics of the system relative to its equilibrium point is consistent with the fact that the

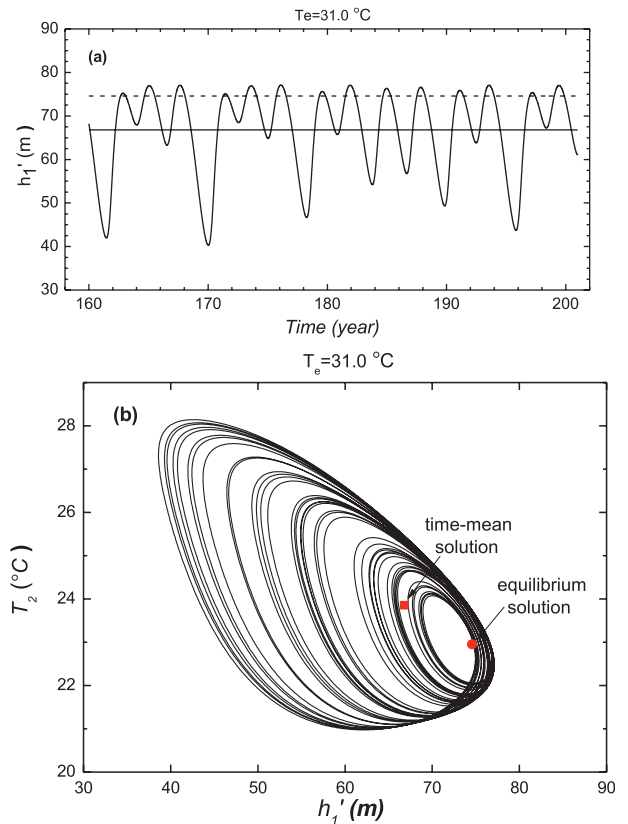


FIG. 6. (a) The time series of h_1' , corresponding to the time series of T_2 shown in Fig. 5b. The time mean value and the equilibrium value of h_1' are also plotted in the figure; see the solid and dashed horizontal lines. (b) The corresponding trajectory of the system, projected onto the plan of T_2 and h_1' . The small red circle and square in the figure mark the positions of the equilibrium and time-mean state, respectively.

Hopf bifurcation (an instability) that brings the oscillation into being takes place *only* when the equilibrium state has a zonal SST contrast that is sufficiently strong, and a depth of thermocline in the western Pacific that is sufficiently deep. In a sense, the zonal SST contrast may be regarded as the thermal stress actually “felt” by the system, and the Hopf bifurcation (an instability) takes place when this “stress” is too strong to bear. After breaking away from the equilibrium point through an instability, the system finds itself mostly on the more stable (or less stressful) side of its phase space—leading to a warmer eastern Pacific (and a reduced zonal SST contrast)—on average. This insight into the nature of ENSO—its asymmetry and its contribution to the time-mean state—will not be easily obtained if we do not subject the system to a gradually varying external thermal forcing as we have done here. In the next section, we explore which nonlinearity in the system enables it to be capable of this seemingly “purposeful” behavior.

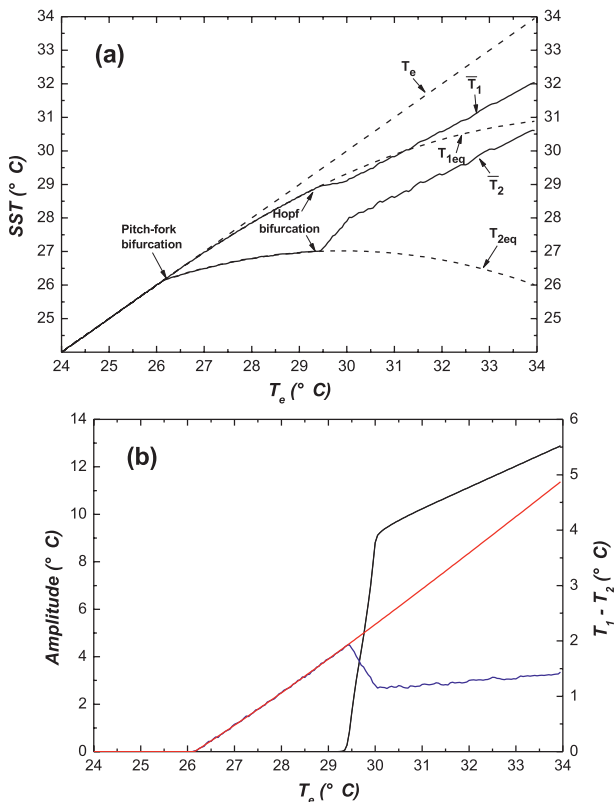


FIG. 7. As in Figs. 2a and 2b, but with the reference profile used to parameterize the subsurface temperature T_{sub} [Eq. (6)] replaced by $\Phi(z) = T_{s0} + \gamma(z + H_1)$, where $T_{s0} = \lambda T_e + (1 - \lambda)T_b$ and $\gamma = (T_e - T_b)/2H_{\text{ref}}$. Parameter values used for this the linear profile are $\lambda = 17/24$ and $H_{\text{ref}} = 64$ m. Other parameters are as in Fig. 2.

5. The nonlinearity responsible for rectification

In addition to the nonlinear advection term in the system [the second term on the right-hand side of Eq. (2)], there is another source of nonlinearity—the reference temperature profile for the subsurface ocean [Eq. (6)] used to parameterize T_{sub} [Eq. (5)]. When a linear profile is used, the rectification effect of ENSO events is found to be equally profound (Figs. 7a,b), indicating that it is the nonlinear advection term on the right-hand side of Eq. (2) that provides the underlying mechanism for the rectification effect.

The linear profile used to obtain Fig. 7 is the same used in the stability analysis of Sun (1997, 2000):

$$\Phi(z) = T_{s0} + \gamma(z + H_1), \quad (9)$$

where $T_{s0} = \lambda T_e + (1 - \lambda)T_b$ and $\gamma = (T_e - T_b)/2H_{\text{ref}}$, λ is a numerical constant. Note that H_{ref} has the dimension of depth. The corresponding Eq. (5) becomes

$$T_{\text{sub}} = T_{s0} + \gamma h_2'. \quad (10)$$

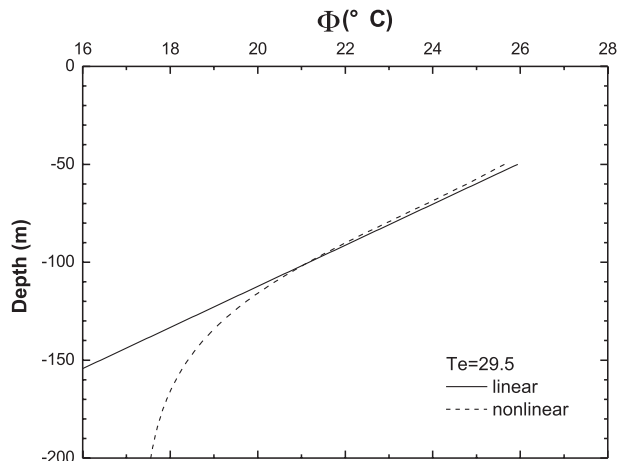


FIG. 8. The profile for the reference subsurface temperature used to link the subsurface temperature to the depth of the thermocline for the linear case (solid; Fig. 7) and the nonlinear case (dashed; Fig. 2). Only the profile corresponding to $T_e = 29.5^\circ\text{C}$ is plotted here.

Figure 7 shows the results corresponding to Fig. 2, but now with the linear profile Eq. (9) used to parameterize T_{sub} [Eq. (10)]. As anticipated from the stability analysis of Sun (2000), the system with a linear profile undergoes the same regime transitions as the one with a nonlinear profile. As the value of T_e progressively increases, the system first experience a pitchfork bifurcation to create first the zonal SST contrast, and then a Hopf bifurcation when the zonal SST is sufficiently large. The system then starts to oscillate and the time-mean solution and the equilibrium solution start to diverge. It is evident that the warming effect of ENSO events on the eastern Pacific time-mean state is just as profound in Fig. 7 as in Fig. 2. There are quantitative differences between Figs. 2 and 7 even in the region immediately following the Hopf bifurcation. Figure 8 contrasts the nonlinear profile with the linear profile at $T_e = 29.5^\circ\text{C}$. Note that the two profiles have slightly different slopes even in the region in the upper part of the thermocline. The constants used in defining the linear profile are tuned to get a Hopf bifurcation point that is close to that with the tangent profile, not to match the lapse rate implied from the tangent profile at any particular depth.

With Eq. (9) replacing Eq. (6), it has been shown in Sun (2000) that the dynamic behavior of the system is controlled by the following four nondimensional parameters: s , R , Λ , and σ , with the latter three parameters given as (see appendix B for details)

$$R = \frac{\alpha(T_e - T_{s0})}{ac}, \quad (11)$$

$$\Lambda = p\kappa\gamma^*, \quad \text{and} \quad (12)$$

$$\sigma = \frac{r}{c}, \quad (13)$$

where $p = (H_1/2H_2)[1 + (H_1/H_2)]$, $\kappa = ac/b^2$, $b = c_k/L_x$, with c_k being the phase speed of the first baroclinic Kelvin wave and L_x is the half of the zonal width of the basin, and $\gamma^* = \gamma/\gamma_0$, with $\gamma_0 = (T_e - T_{s0})/H_2$. (For convenience of reference, appendix A lists the definition of all the symbols and parameters used in this article.)

An exhaustive numerical exploration of the rectification effect in the entire parameter space is beyond the scope of the present study. We only present two situations here in which an analytical form for the rectification effect can be obtained to underscore the fundamental importance of the nonlinear advection term in Eq. (2) in giving rise to this effect. The details of the derivations are given in appendix C.

With $s = 0$, $\sigma = (r/c) \gg 1$, it can be shown that

$$\overline{T_1} \approx T_{1\text{eq}} \quad \text{and} \quad (14)$$

$$\overline{T_2} \approx T_{2\text{eq}} + \frac{\overline{T_2'^2}}{T_1 - T_2}, \quad (15)$$

where the overbar refers to the time mean, eq refers to equilibrium, and the prime denotes the anomaly above the time mean. (Details of derivation are given in appendix C.) Equation (15) links the refraction effect—the difference between the time-mean T_2 and the equilibrium $T_{2\text{eq}}$ —to the variance of the anomaly about the time mean—the level of ENSO activity.

The simplest advective case (or convective case) (Fig. 9)—the situation considered in Sun (2000) and Schopf and Burgman (2006) as a thought experiment in which the eastern Pacific is periodically (or episodically with a 50% frequency) flooded by warm water due to an expanding warm pool—appears to satisfy Eq. (15). In that situation, $\overline{T_1} \sim T_{1\text{eq}}$, $\overline{T_2} \sim (1/2)(T_{1\text{eq}} + T_{2\text{eq}})$, and $\overline{T_2'} \sim \overline{T_1} - \overline{T_2} \approx (1/2)(T_{1\text{eq}} - T_{2\text{eq}})$, with $\overline{T_2'}$ being a measure of the magnitude of T_2' (the anomaly about the time mean).

For a more general value of σ , but with $\Lambda R \gg 1$, we have

$$\overline{T_2} \approx T_{2\text{eq}} + \frac{\overline{T_2'^2}}{T_1 - T_2} \cos\beta, \quad (16)$$

where β is the phase difference between T_{sub} and T_2 . The details of derivation are provided in appendix C. Note that $\Lambda R \gg 1$ corresponds to a situation with strong Bjerknes feedback, because

$$\Lambda R = \frac{H_1}{2H_2} H \frac{\alpha\gamma}{b^2}. \quad (17)$$

Recall that α and γ in Eq. (17) are respectively the coupling strength and the lapse rate of the thermocline (see appendix A).

Presenting Eqs. (15) and (16) here is to further show that the rectification effect appears to be a robust property of the nonlinearity in Eq. (2) and at least qualitatively does not appear to be sensitive to the choice of parameters.

6. Summary and discussion

Motivated by a need for a more complete understanding about the observed co-occurrences of an elevated (reduced) level of ENSO activity and a background warming (cooling) in the eastern tropical Pacific, we have employed a novel methodology to delineate the effect of ENSO events on the time-mean equatorial upper ocean. This new methodology is to contrast the time-mean state of a low-order nonlinear model with its equilibrium state. The realized time-dependent state in this model is calculated numerically, and the corresponding equilibrium state is obtained analytically, allowing us to compare the two states of coupled equatorial Pacific side by side, and thereby delineate the role of ENSO in shaping the tropical Pacific climatology.

The results from such an exercise show unambiguously that in the presence of ENSO, the differences between the equilibrium state and the realized time-mean state are significant. In particular, it is found that the time-mean equatorial eastern Pacific SST is significantly higher than that in the equilibrium state and that the time-mean zonal SST contrast is significantly weaker than that in the equilibrium state. The differences between the two states are further shown numerically to be proportional to the magnitude of ENSO oscillation.

The present results advance our understanding of the effect of ENSO events on the time-mean equatorial ocean beyond that gained from empirical studies (e.g., Rodgers et al. 2004; Sun and Yu 2009). This result, together with that from Sun and Zhang (2006) and Schopf and Burgman (2006), adds weight to the argument that the recent decadal warming in the eastern tropical Pacific may be a consequence of the elevation of ENSO events during this period.

Although the present results strengthen the argument that the recent decadal warming in the eastern tropical Pacific may be a consequence of the elevation of ENSO events during this period, such a causality cannot be firmly established unless the causes of the elevation of ENSO activity are shown to be independent of the

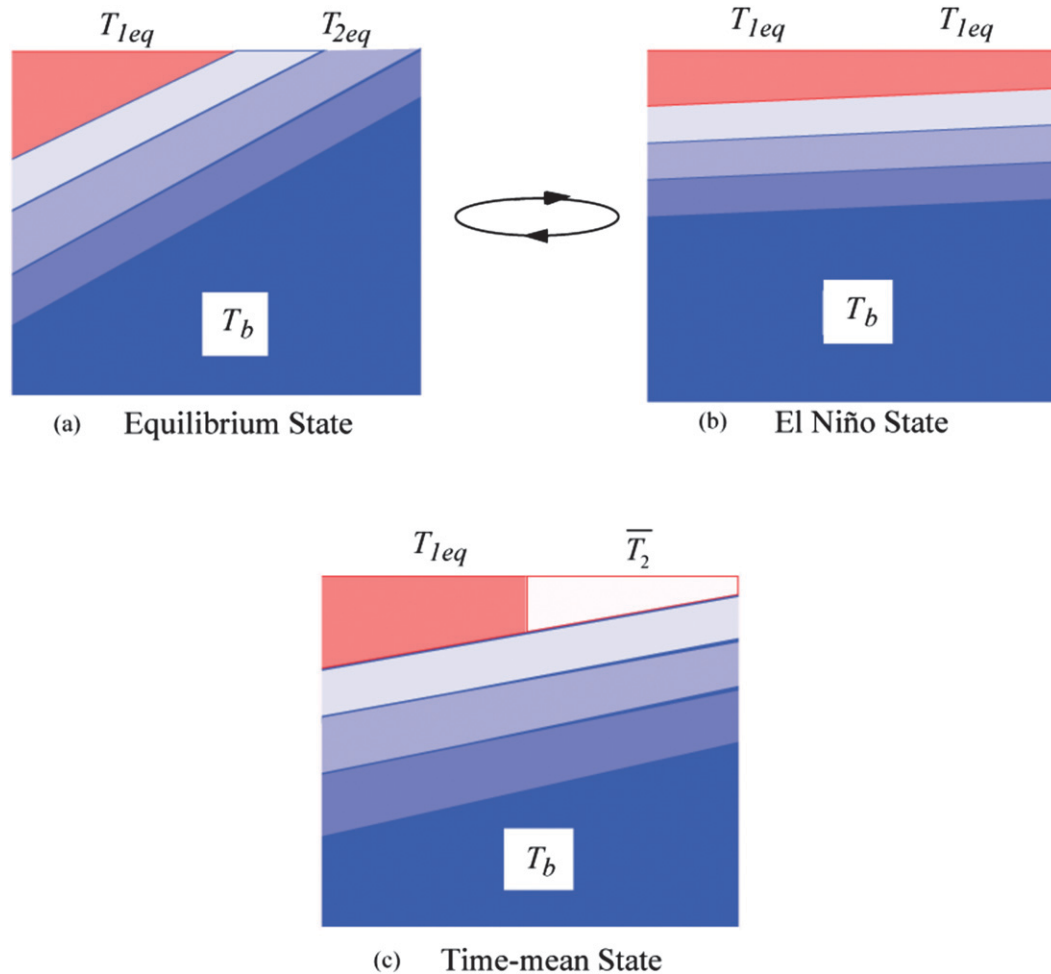


FIG. 9. (a),(b) A schematic illustration of the simple advective model in which El Niño event is viewed as a periodic (or episodic) “flooding” event of the eastern Pacific region—a region that is otherwise cold (when instability does not take place)—by warm water in the western Pacific. (c) The resulting time-mean state. In the situation of a sinusoidal expansion of the warm pool, $\bar{T}_1 \sim T_{1eq}$, $\bar{T}_2 \sim (1/2)(T_{1eq} + T_{2eq})$, and $\bar{T}'_2 \sim \bar{T}_1 - \bar{T}_2 = (1/2)(T_{1eq} - T_{2eq})$, with \bar{T}'_2 being the magnitude of T'_2 or ENSO anomaly.

decadal background warming in the tropical Pacific. As earlier studies have shown that a decadal warming in the background state can cause an elevation of ENSO activity (Fedorov and Philander 2000, 2001; An and Jin 2001; Wang and An 2001), the possibility is raised that a nonlinear interaction between ENSO events and the time-mean state may act as a viable mechanism for decadal variability in the tropical Pacific region. We note, however, the study by Wittenberg (2009) that shows that the level of ENSO activity in a GFDL model can change substantially from one decadal epoch to another without any notable change in the time-mean state over the epoch. We agree that there may be other causes for decadal variability in the level of ENSO activity, such as random forcing from weather events. An interesting venue to pursue is how the collective effect of weather events over

the warm pool influences the decadal variability in the tropical maximum SST and thereby the decadal variability in the value of T_e . We may not be able to conclude that the apparent lack of rectification of the mean state in the GFDL model contradicts our conclusions here also before we fully assess whether the ENSO events in the model are too linear relative to what we see in observations (Y. Sun et al. 2011, unpublished manuscript). In fully assessing ENSO asymmetry, it is important to examine its subsurface signatures (Zhang et al. 2009).

The analytical model also shows that at least in certain regimes, the amplitude of ENSO events increases with enhanced radiative heating. Thus an interesting emerging scenario is that ENSO events become stronger in response to an enhanced radiative heating, which causes a warming in the tropical Pacific. Such a scenario is not

supported by coupled GCM simulations, however. A survey of coupled GCM simulations has not revealed any systematic change in the level of ENSO activity in response to global warming (Collins et al. 2010). This apparent contradiction may be again due to the fact that the nonlinearity of ENSO is either nonexistent or severely underestimated by coupled GCMs (An et al. 2005; Sun 2010; Y. Sun et al. 2011, unpublished manuscript). Related to this consideration is the question of whether the tropical Pacific region in the coupled GCMs is in the same dynamic regime as in the real world (Sun et al. 2006; Guilyardi et al. 2009, 2012). It is also possible that the present model is too simple. A key issue ahead is to bridge the gap between simple models and GCMs in their predictions of the response of ENSO to global warming. Addressing this issue may necessarily entail a more critical assessment of the nonlinearity of ENSO events in the models including a quantification of the rectification effect of ENSO into the mean state in the various GCMs.

The results from the present analysis also suggest that the sensitivity of the tropical Pacific mean climate, the zonal SST contrast in particular, to an increase in the greenhouse effect may be a function of the time-mean effect of ENSO events. The reduced rate of increase in the time-mean zonal SST contrast ($T_1 - T_2$) in the present model in response to an increase in the radiative–convective equilibrium SST (T_e), compared to that in the equilibrium state, suggests that the zonal SST contrast may be regulated by ENSO events. Whether this provides a viable explanation for the difficulty of detecting a significant trend in the zonal SST contrast in the observations discussed by Vecchi et al. (2008) is a question worth exploring. In the same vein, recognizing this nonlinear effect of ENSO and the apparent inability to fully capture this effect by all the models may prove useful for fully understanding the differences among model predictions of the response of the zonal SST contrast to global warming. The results thus underscore the importance for climate models to correctly simulate ENSO, and its nonlinear dynamics in particular, in order to capture correctly the response of the ENSO and the climatological state it determines.

We would like to note that the results reported in this article are from a highly truncated version of the real coupled tropical Pacific ocean–atmosphere system. A salient feature in the decadal warming of the east tropical Pacific (Fig. 1) is that the maximum warming is not right on the equator. But the model in its current form does not carry any information about the meridional structure of the rectification effect. The results will have to be compared with those obtained by more sophisticated models in order to fully ascertain the time-mean

effect of ENSO events. Regardless of the accuracy of the present results, the framework they constitute is likely to be useful for diagnosing and understanding the results from more complicated climate models, such as GCMs.

It has been suggested that ENSO variability may be simulated by a stable linear system forced by weather noise (Penland and Sardeshmukh 1995; Penland 1996; Moore and Kleeman 1999; Flugel et al. 2004; Kleeman 2008, among others). Indeed, these models have performed remarkably well in simulating the SST anomalies associated with ENSO events. Hence the debate as to whether ENSO dynamics is “linear” or “nonlinear.” It has been often overlooked, however, that these studies take the stability of the time-mean state as a given and do not address the question of why the time-mean state appears to be subcritical. The present study may have accidentally addressed this question and provided a potential underpinning for these studies using anomaly models. An emerging narrative from the present study is that ENSO events result from an instability of the equilibrium state and, through their time-mean effect, create a time-mean state that is subcritical when measured by the eigenvalues of a linear system obtained by linearizing the original system about its time-mean state. A subsequent study is planned to test this hypothesis more quantitatively. We will force the linear system constituted by the time-mean variables with weather noise to bridge the present work quantitatively with those studies underscoring the role of noise in the irregularity of ENSO. With weather noise included, we will also run the present nonlinear model in a stable regime or at its critical point to see whether the interannual variability resulting from the forcing from weather events will create a more stable time-mean state. For now, the results from this simple nonlinear model will help to underscore the fact that the equilibrium state of the coupled tropical ocean–atmosphere may not be the same as its time-mean state (i.e., the climatological state). With this difference in mind, we are hopeful that the gap between the two schools of thoughts about the nature of ENSO dynamics may turn out to be not that big after all.

Acknowledgments. The authors thank University of Colorado at Boulder for hosting Jin Liang for his visit. The research was supported by the National Natural Science Foundation of China (NSFC) under Grants 40730953 and 40805025, and by U.S. NSF Grant AGS 0852329 (Climate and Large-Scale Dynamics Program) and by grants from NOAA office of global programs (Earth System Science Program and Modeling, Analysis, Prediction, and Projection Program). We thank the three anonymous reviewers and the editor for their very helpful questions and suggestions.

APPENDIX A

Definition of the Symbols Used in this Study

T_e	the radiative–convective equilibrium temperature
T_b	deep ocean temperature
T_1	equatorial western Pacific SST (120°E–155°W)
T_2	equatorial eastern Pacific SST (155°–70°W)
T_{sub}	subsurface temperature
H_1	depth of the mixed layer
H	zonal mean depth of the upper ocean ($H_2 = H - H_1$)
L_x	half-width of the basin
u	zonal velocity
w	upwelling velocity
q	w/H_1
s	uH_1/wL_x
$1/a$	adjustment time scale of the surface ocean currents to changes in the surface winds
$1/c$	time scale of removing a SST anomaly by surface fluxes
$1/r$	time scale of the slow adjustment in the ocean
α	sensitivity of the surface wind stress to changes in the SST gradients
h'_1	deviation of the depth of the upper ocean in the western Pacific from its reference value H
h'_2	deviation of the depth of the upper ocean in the eastern Pacific from its reference value H
c_k	phase speed of the first baroclinic Kelvin wave
b	c_k/L_x
p	$H_1/2H_2(1 + H_1/H_2)$
κ	ac/b^2
σ	r/c
T_{s0}	characteristic value of the subsurface temperature
λ	parameter used to link T_{s0} with T_e and T_b through a linear extrapolation.
γ	lapse rate of the subsurface ocean
γ_0	$(T_e - T_{s0})/H_2$, a reference lapse rate for the subsurface ocean.
γ^*	γ/γ_0
R	$\alpha(T_e - T_{s0})ac$
Λ	$p\kappa\gamma^*$

APPENDIX B

A Nondimensional Analysis of the Dynamic System

With the nonlinear profile shown in Eq. (6) replaced by a linear profile shown in Eq. (9), the equations governing the behavior of the system are

$$\frac{dT_1}{dt} = c(T_e - T_1) + sq(T_2 - T_1), \quad (\text{B1})$$

$$\frac{dT_2}{dt} = c(T_e - T_2) + q(T_{\text{sub}} - T_2), \quad (\text{B2})$$

$$q = \frac{\alpha}{a}(T_1 - T_2), \quad (\text{B3})$$

$$T_{\text{sub}} = T_{s0} + \gamma h'_2, \quad (\text{B4})$$

$$T_{s0} = \lambda T_e + (1 - \lambda)T_b, \quad (\text{B5})$$

$$\gamma = \gamma^* \frac{T_e - T_{s0}}{H_2}, \quad (\text{B6})$$

$$h'_2 - h'_1 = -\frac{H_1 H}{H_2} \frac{\alpha}{b^2} (T_1 - T_2), \quad \text{and} \quad (\text{B7})$$

$$\frac{1}{r} \frac{dh'_1}{dt} = -h'_1 + \frac{H_1}{2H_2} H \frac{\alpha}{b^2} (T_1 - T_2). \quad (\text{B8})$$

By introducing $\tau = ct$, $T_1^* = (T_1 - T_e)/(T_e - T_{s0})$, $T_2^* = (T_2 - T_e)/(T_e - T_{s0})$, $T_s^* = (T_{\text{sub}} - T_e)/(T_e - T_{s0})$, $q^* = q/c$, $\gamma^* = \gamma H_2/(T_e - T_{s0})$, $h'_1{}^* = h'_1/H_2$, and $h'_2{}^* = h'_2/H_2$, we have the nondimensional form of (B1)–(B8) as

$$\frac{dT_1^*}{d\tau} = -T_1^* + sq^*(T_2^* - T_1^*), \quad (\text{B9})$$

$$\frac{dT_2^*}{d\tau} = -T_2^* + q^*(T_s^* - T_2^*), \quad (\text{B10})$$

$$\frac{dh'_1{}^*}{d\tau} = -\sigma[h'_1{}^* - p\kappa R(T_1^* - T_2^*)], \quad (\text{B11})$$

$$q^* = R(T_1^* - T_2^*), \quad (\text{B12})$$

$$T_s^* = -1 + \gamma^* h'_2{}^*, \quad \text{and} \quad (\text{B13})$$

$$h'_2{}^* = h'_1{}^* - 2p\kappa R(T_1^* - T_2^*), \quad (\text{B14})$$

where $R = \alpha(T_e - T_{s0})/ac$, $\kappa = ac/b^2$, $\sigma = r/c$, and $p = H_1/2H_2(1 + H_1/H_2)$. Plugging (B12)–(B14) into (B9)–(B11), and replacing $\gamma^* h'_1{}^*$ by η_1^* and $\gamma^* h'_2{}^*$ by η_2^* , we have

$$\frac{dT_1^*}{d\tau} = -T_1^* - sR(T_2^* - T_1^*)^2, \quad (\text{B15})$$

$$\begin{aligned} \frac{dT_2^*}{d\tau} = & -T_2^* + R(T_1^* - T_2^*)[-1 + \eta^* \\ & - 2\Lambda R(T_1^* - T_2^*) - T_2^*], \end{aligned} \quad (\text{B16})$$

$$\frac{1}{\sigma} \frac{d\eta_1^*}{d\tau} = -\eta_1^* + \Lambda R(T_1^* - T_2^*), \quad (\text{B17})$$

$$T_s^* = -1 + \eta_2^*, \quad \text{and} \quad (\text{B18})$$

$$\eta_2^* = \eta_1^* - 2\Lambda R(T_1^* - T_2^*), \quad (\text{B19})$$

where $\Lambda = \rho\kappa\gamma^*$. After such a manipulation to consolidate the parameters, we see that the dynamic behavior of the coupled system is determined by four non-dimensional parameters: R , Λ , σ , and s .

APPENDIX C

An Analysis of the Relationship among the Time-Mean Solution, the Equilibrium Solution, and the Amplitude of the Anomaly about the Time Mean

a. The equilibrium solutions

The equilibrium solutions can be obtained by setting the time derivatives on the left-hand sides of (B1), (B2), and (B8) to zero, and then reducing (B1)–(B8) to a single nonlinear algebraic equation. Here we only present the case for $s = 0$. With $s = 0$, (B1)–(B8) can be rewritten as

$$T_{1\text{eq}} = T_e, \quad (\text{C1})$$

$$c(T_e - T_{2\text{eq}}) + \frac{\alpha}{a}(T_{1\text{eq}} - T_{2\text{eq}}) \times (T_{s0} + \gamma^* \frac{T_e - T_{s0}}{H_2} h'_{2\text{eq}} - T_{2\text{eq}}) = 0, \quad (\text{C2})$$

$$q_{\text{eq}} = \frac{\alpha}{a}(T_{1\text{eq}} - T_{2\text{eq}}), \quad (\text{C3})$$

$$h'_{2\text{eq}} = -\frac{H_1}{2H_2} H \frac{\alpha}{b^2} (T_{1\text{eq}} - T_{2\text{eq}}), \quad \text{and} \quad (\text{C4})$$

$$h'_{1\text{eq}} = \frac{H_1}{2H_2} H \frac{\alpha}{b^2} (T_{1\text{eq}} - T_{2\text{eq}}). \quad (\text{C5})$$

(The subscript eq denotes the corresponding equilibrium solution of each variable.)

Plugging (C1) and (C4) into Eq. (C2), we have

$$c(T_e - T_{2\text{eq}}) + \frac{\alpha}{a}(T_e - T_{2\text{eq}}) \times \left[T_{s0} + \gamma^* \frac{T_e - T_{s0}}{H_2} - \frac{H_1}{2H_2} H \frac{\alpha}{b^2} (T_e - T_{2\text{eq}}) - T_{2\text{eq}} \right] = 0$$

$$\rightarrow \frac{ac}{\alpha} + T_{s0} + \gamma^* \frac{T_e - T_{s0}}{H_2} - \frac{H_1}{2H_2} H \frac{\alpha}{b^2} (T_{2\text{eq}} - T_e) - T_{2\text{eq}} = 0. \quad (\text{C6})$$

By introducing the nondimensional parameters R , Λ , p , κ , and σ , (C6) can be rewritten as

$$\frac{ac}{\alpha} + T_{s0} + \Lambda R(T_{2\text{eq}} - T_e) - T_{2\text{eq}} = 0$$

$$\rightarrow T_{2\text{eq}} = \frac{\frac{ac}{\alpha} + T_{s0} - \Lambda R T_e}{1 - \Lambda R}. \quad (\text{C7})$$

Equations (C1) and (C7) are the equilibrium solutions of the linear system.

b. Relationship among the time-mean solution, the equilibrium solution, and the amplitude of the anomaly about the time mean

Because a variable (e.g., T) in its oscillatory state can be decomposed into its climatological mean (\bar{T}) and corresponding fluctuating part (T'), the western and eastern equatorial Pacific SST can be respectively written as $T_1 = \bar{T}_1 + T'_1$ and $T_2 = \bar{T}_2 + T'_2$ (also $h'_2 = \bar{h}'_2 + h''_2$). The difference between the two solutions can be expressed either in the dimensional or nondimensional form. Here we only present the derivation in the dimensional form, and only refer the nondimensional form of the equations when asymptotic approximation is needed to obtain a clearer relation among the time-mean value, the equilibrium value, and the amplitude of the anomalies about the time mean.

After we time averaging to the two sides of (B1), (B2), (B7), and (B8) in the case $s = 0$, and combine Eqs. (B3)–(B6), then we have

$$\frac{dT_1}{dt} = c(T_e - T_1), \quad (\text{C8})$$

$$\frac{dT_2}{dt} = c(T_e - T_2) + \frac{\alpha}{a}(T_1 - T_2)(T_{s0} + \gamma h'_2 - T_2), \quad (\text{C9})$$

$$\bar{h}'_2 - \bar{h}'_1 = -\frac{H_1}{H_2} H \frac{\alpha}{b^2} (\bar{T}_1 - \bar{T}_2), \quad \text{and} \quad (\text{C10})$$

$$\frac{1}{r} \frac{dh'_1}{dt} = -\bar{h}'_1 + \frac{H_1}{2H_2} H \frac{\alpha}{b^2} (\bar{T}_1 - \bar{T}_2). \quad (\text{C11})$$

Simplifying (C8)–(C11), we can get

$$\bar{T}_1 = T_e, \quad (\text{C12})$$

$$c(T_e - T_2) + \frac{\alpha}{a}(T_1 - T_2)(T_{s0} + \gamma h'_2 - T_2) = 0, \quad (\text{C13})$$

$$\bar{h}'_2 = -\frac{H_1}{2H_2} H \frac{\alpha}{b^2} (\bar{T}_1 - \bar{T}_2), \quad \text{and} \quad (\text{C14})$$

$$\bar{h}'_1 = \frac{H_1}{2H_2} H \frac{\alpha}{b^2} (\bar{T}_1 - \bar{T}_2). \quad (\text{C15})$$

Simplifying (C13), we have

$$\begin{aligned}
cT_e - c\bar{T}_2 + \frac{\alpha}{a}(\bar{T}_1 - \bar{T}_2 + T_1' - T_2')(T_{s0} + \gamma\bar{h}_2' - \bar{T}_2 + \gamma h_2'' - T_2') &= 0 \\
\rightarrow \frac{ac}{\alpha}(T_e - \bar{T}_2) + [(\bar{T}_1 - \bar{T}_2)(T_{s0} + \gamma\bar{h}_2' - \bar{T}_2) + (T_1' - T_2')(\gamma h_2'' - T_2')] &= 0. \quad (C16)
\end{aligned}$$

As we can easily get $\bar{T}_1 = T_{\text{eq}} = T_e$ from a combination of (C1) and (C12), and there is no oscillation for T_1 at this time, $T_1' = 0$. Also by combining (C14), Eq. (C16) can be further simplified as

$$\begin{aligned}
\frac{ac}{\alpha}(T_e - \bar{T}_2) + (T_e - \bar{T}_2) \left[T_{s0} + \gamma^* \frac{T_e - T_{s0} - H_1}{H_2} H \frac{\alpha}{b^2} (\bar{T}_1 - \bar{T}_2) - \bar{T}_2 \right] + \overline{(-T_2')(\gamma h_2'' - T_2')} &= 0 \\
\rightarrow \frac{ac}{\alpha}(T_e - \bar{T}_2) + (T_e - \bar{T}_2)(T_{s0} + \Lambda R(\bar{T}_2 - T_e) - \bar{T}_2) + \overline{(-T_2')(\gamma h_2'' - T_2')} &= 0 \\
\rightarrow \frac{ac}{\alpha} + T_{s0} + (\Lambda R - 1)\bar{T}_2 - \Lambda R T_e + \frac{\overline{(-T_2')(\gamma h_2'' - T_2')}}{T_e - \bar{T}_2} &= 0 \\
\rightarrow \bar{T}_2 = \frac{\frac{ac}{\alpha} + T_{s0} - \Lambda R T_e}{1 - \Lambda R} + \frac{\overline{\gamma h_2'' T_2' - T_2'^2}}{(\Lambda R - 1)(T_e - \bar{T}_2)}. \quad (C17)
\end{aligned}$$

As shown by (C7), $T_{2\text{eq}} = \{(ac/\alpha) + [T_{s0} - \Lambda R T_e]\} / (1 - \Lambda R)$, the relationship between \bar{T}_2 and $T_{2\text{eq}}$ is

$$\bar{T}_2 = T_{2\text{eq}} + \frac{\overline{\gamma h_2'' T_2' - T_2'^2}}{(\Lambda R - 1)(T_e - \bar{T}_2)}. \quad (C18)$$

As we get easily get $T_{\text{sub}}' = \gamma h_2''$ [recall that $T_{\text{sub}} = T_{s0} + \gamma h_2'$; (B4)], (C18) can be rewritten as

$$\bar{T}_2 = T_{2\text{eq}} + \frac{\overline{T_{\text{sub}}' T_2' - T_2'^2}}{(\Lambda R - 1)(T_e - \bar{T}_2)}. \quad (C19)$$

When $\sigma = (r/c) \gg 1$, Eq. (B17) becomes $\eta_1^* = \Lambda R(T_1^* - T_2^*)$. As $T_1^* = 0$ ($s = 0$) at this time, by combining Eqs. (B18) and (B19) we can get $T_2^* + 1 = \Lambda R T_2^*$. We can further get $T_{\text{sub}}' = \Lambda R T_2'$ easily as we return it to its dimensional form. Equation (C19) can thereby be derived as

$$\bar{T}_2 = T_{2\text{eq}} + \frac{\overline{T_2'^2}}{T_e - \bar{T}_2}. \quad (C20)$$

Recall that in this particular case, $\bar{T}_1 = T_e$, we have

$$\bar{T}_2 = T_{2\text{eq}} + \frac{\overline{T_2'^2}}{T_1 - \bar{T}_2}. \quad (C21)$$

The simple advective case (that the eastern Pacific is periodically invaded or flooded by an expanding warm pool; Fig. 9) appears to satisfy this equation, with $\tilde{T}_2' \sim \bar{T}_1 - \bar{T}_2 = (1/2)(T_{1\text{eq}} - T_{2\text{eq}})$, $\bar{T}_1 \sim T_{1\text{eq}}$, and $\bar{T}_2 \sim (1/2)(T_{1\text{eq}} + T_{2\text{eq}})$, where \tilde{T}_2' is the magnitude of the anomaly above the time mean.

For a more general case, we take $T_2' = A \cos \omega t$, $T_{\text{sub}}' = \Lambda R A \cos(\omega t - \beta)$ ($\beta > 0$),

$$\begin{aligned}
T_{\text{sub}}' T_2' &= \Lambda R [A^2 \cos \omega t \cos(\omega t - \beta)] \\
&= \Lambda R [A^2 \cos \omega t (\cos \omega t \cos \beta + \sin \omega t \sin \beta)] \\
&= \Lambda R [A^2 \cos^2 \omega t \cos \beta + A^2 \cos \omega t \sin \omega t \sin \beta],
\end{aligned}$$

and

$$\overline{T_{\text{sub}}' T_2'} = \Lambda R A^2 \overline{\cos^2 \omega t \cos \beta} = \Lambda R \cos \beta \overline{T_2'^2}.$$

Equation (C19) becomes

$$\bar{T}_2 = T_{2\text{eq}} + \frac{\Lambda R \cos \beta - 1}{\Lambda R - 1} \frac{\overline{T_2'^2}}{T_1 - \bar{T}_2}. \quad (C22)$$

When $\Lambda R \gg 1$, Eq. (C22) becomes

$$\bar{T}_2 = T_{2\text{eq}} + \cos \beta \frac{\overline{T_2'^2}}{T_1 - \bar{T}_2}. \quad (C23)$$

Note that

$$\begin{aligned}
\Lambda R &= p\kappa\gamma^*R \\
&= (H_1/2H_2)(1 + [H_1/H_2]) \cdot \frac{ac}{b^2} \cdot \frac{\gamma H_2}{T_e - T_{s0}} \cdot \alpha \frac{T_e - T_{s0}}{ac} \\
&= \frac{H_1 H \alpha \gamma}{2H_2 b^2}. \quad (C24)
\end{aligned}$$

Therefore, (C23) corresponds to the case with a very strong Bjerknes feedback. Recall that α and γ in (C24)

are respectively the coupling strength and the lapse rate of the thermocline (appendix A).

REFERENCES

- An, S.-I., and F.-F. Jin, 2001: Collective role of thermocline and zonal advective feedbacks in the ENSO mode. *J. Climate*, **14**, 3421–3432.
- , and —, 2004: Nonlinearity and asymmetry of ENSO. *J. Climate*, **17**, 2399–2412.
- , Y.-G. Ham, J.-S. Kug, F.-F. Jin, and I.-S. Kang, 2005: El Niño–La Niña asymmetry in the Coupled Model Intercomparison Project simulations. *J. Climate*, **18**, 2617–2627.
- Burgers, G., and D. B. Stephenson, 1999: The “normality” of El Niño. *Geophys. Res. Lett.*, **26**, 1027–1030, doi:10.1029/1999GL900161.
- Cane, M. A., A. C. Clement, A. Kaplan, Y. Kushnir, D. Pozdnyakov, R. Seager, S. E. Zebiak, and R. Murtugudde, 1997: Twentieth-century sea surface temperature trends. *Science*, **275**, 957–960.
- Clement, A. C., R. Seager, M. A. Cane, and S. E. Zebiak, 1996: An ocean dynamical thermostat. *J. Climate*, **9**, 2190–2196.
- Collins, M., and Coauthors, 2010: The impact of global warming on the tropical Pacific Ocean and El Niño. *Nat. Geosci.*, **3**, 391–397.
- Deng, L., X.-Q. Yang, and Q. Xie, 2010: ENSO frequency change in coupled climate models as response to the increasing CO₂ concentration. *Chin. Sci. Bull.*, **55**, 744–751.
- Fedorov, A. V., and S. G. Philander, 2000: Is El Niño changing? *Science*, **288**, 1997–2002.
- , and —, 2001: A stability analysis of tropical ocean–atmosphere interactions: Bridging measurements and theory for El Niño. *J. Climate*, **14**, 3086–3101.
- Flugel, M., P. Chang, and C. Penland, 2004: Identification of dynamical regimes in an intermediate coupled ocean–atmosphere model. *J. Climate*, **13**, 2105–2115.
- Gent, P. R., and M. A. Cane, 1989: A reduced gravity, primitive equation model of the upper equatorial ocean. *J. Comput. Phys.*, **81**, 444–480.
- Guilyardi, E., A. Wittenberg, A. Fedorov, M. Collins, C. Wang, A. Capotondi, G. J. van Oldenborgh, and T. Stockdale, 2009: Understanding El Niño in ocean–atmosphere general circulation models. *Bull. Amer. Meteor. Soc.*, **90**, 325–340.
- , W. J. Cai, M. Collins, A. Fedorov, F.-F. Jin, A. Kumar, D.-Z. Sun, and A. Wittenberg, 2012: New strategies for evaluating ENSO processes in climate models. *Bull. Amer. Meteor. Soc.*, **93**, 235–238.
- Jin, F.-F., 1996: Tropical ocean–atmosphere interaction, Pacific cold tongue, and El Niño–Southern Oscillation. *Science*, **274**, 76–78.
- , 1997: An equatorial ocean recharge paradigm for ENSO. Part I: Conceptual model. *J. Atmos. Sci.*, **54**, 811–829.
- , S.-I. An, A. Timmermann, and J. X. Zhao, 2003: Strong El Niño events and nonlinear dynamical heating. *Geophys. Res. Lett.*, **30**, 1120, doi:10.1029/2002GL016356.
- Kleeman, R., 2008: Stochastic theories for the irregularity of ENSO. *Philos. Trans. Roy. Soc.*, **366A**, 2509–2524.
- Manabe, S., and R. F. Möller, 1961: On the radiative equilibrium and the heat balance of the atmosphere. *Mon. Wea. Rev.*, **89**, 503–532.
- , and R. F. Strickler, 1964: Thermal equilibrium of the atmosphere with convective adjustment. *J. Atmos. Sci.*, **21**, 361–385.
- , and R. T. Wetherald, 1967: Thermal equilibrium of the atmosphere with a given distribution of relative humidity. *J. Atmos. Sci.*, **24**, 241–259.
- Meehl, G. A., A. Hu, and C. Tebaldi, 2010: Decadal prediction in the Pacific region. *J. Climate*, **23**, 2959–2973.
- Moore, A., and R. Kleeman, 1999: Stochastic forcing of ENSO by the intraseasonal oscillation. *J. Climate*, **12**, 1199–1220.
- Penland, C., 1996: A stochastic model of Indo-Pacific sea surface temperature anomalies. *Physica D*, **98**, 534–558.
- , and P. D. Sardeshmukh, 1995: The optimal growth of tropical sea surface temperature anomalies. *J. Climate*, **8**, 1999–2024.
- Philander, S. G., 1990: *El Niño, La Niña, and the Southern Oscillation*. Academic Press, 293 pp.
- Picaut, J., F. Masia, and Y. du Penhoat, 1997: An advective-reflective conceptual model for the oscillatory nature of the ENSO. *Science*, **277**, 663–666.
- Rayner, N. A., E. B. Horton, D. E. Parker, C. K. Folland, and R. B. Hackett, 1996: Version 2.2 of the Global Sea-Ice and Sea Surface Temperature data set, 1993–1994. Hadley Centre Climate Research Tech. Note 74 (CRTN74), 46 pp. [Available online at <http://www.metoffice.gov.uk/hadobs/gisst/crtn74.pdf>.]
- Rodgers, K. B., P. Friederichs, and M. Latif, 2004: Tropical Pacific decadal variability and its relation to decadal modulations of ENSO. *J. Climate*, **17**, 3761–3774.
- Schopf, P. S., and R. J. Burgman, 2006: A simple mechanism for ENSO residuals and asymmetry. *J. Climate*, **19**, 3167–3179.
- Strogatz, S., 2001: *Nonlinear Dynamics and Chaos: With Applications to Physics, Biology, Chemistry and Engineering*. Westview Press, 528 pp.
- Sun, D.-Z., 1997: El Niño: A coupled response to radiative heating? *Geophys. Res. Lett.*, **24**, 2031–2034.
- , 2000: Global climate change and ENSO: A theoretical framework. *El Niño: Historical and Paleoclimatic Aspects of the Southern Oscillation, Multiscale Variability, and Global and Regional Impacts*, H. F. Diaz and V. Markgraf, Eds., Cambridge University Press, 443–463.
- , 2003: A possible effect of an increase in the warm-pool SST on the magnitude of El Niño warming. *J. Climate*, **16**, 185–205.
- , 2010: The diabatic and nonlinear aspects of El Niño–Southern Oscillation: Implications for its past and future behavior. *Climate Dynamics: Why Does Climate Vary? Geophys. Monogr.*, Vol. 189, Amer. Geophys. Union, 79–104.
- , and Z. Liu, 1996: Dynamic ocean–atmosphere coupling: A thermostat for the tropics. *Science*, **272**, 1148–1150.
- , and T. Zhang, 2006: A regulatory effect of ENSO on the time-mean thermal stratification of the equatorial upper ocean. *Geophys. Res. Lett.*, **33**, L07710, doi:10.1029/2005GL025296.
- , and Coauthors, 2006: Radiative and dynamical feedbacks over the equatorial cold tongue: Results from nine atmospheric GCMs. *J. Climate*, **19**, 4059–4074.
- Sun, F., and J.-Y. Yu, 2009: A 10–15-yr modulation cycle of ENSO intensity. *J. Climate*, **22**, 1718–1735.
- Timmermann, A., and F.-F. Jin, 2002: A nonlinear mechanism for decadal El Niño amplitude changes. *Geophys. Res. Lett.*, **29**, 1003, doi:10.1029/2001GL013369.
- Vecchi, G. A., A. Clement, and B. J. Soden, 2008: Examining the tropical Pacific’s response to global warming. *Eos, Trans. Amer. Geophys. Union*, **89**, 81, doi:10.1029/2008EO090002.

- Wang, B., and S.-I. An, 2001: Why the properties of El Niño changed during the late 1970s. *Geophys. Res. Lett.*, **28**, 3709–3712.
- Wang, X. L., and C.-F. Ropelewski, 1995: An assessment of ENSO-scale secular variability. *J. Climate*, **8**, 1584–1599.
- Wittenberg, A. T., 2009: Are historical records sufficient to constrain ENSO simulations? *Geophys. Res. Lett.*, **36**, L12702, doi:10.1029/2009GL038710.
- Xu, K.-M., and K. A. Emanuel, 1989: Is the tropical atmosphere conditionally unstable? *Mon. Wea. Rev.*, **117**, 1471–1479.
- Zebiak, S. E., and M. A. Cane, 1987: A model El Niño–Southern Oscillation. *Mon. Wea. Rev.*, **115**, 2262–2278.
- Zhang, T., D.-Z. Sun, R. Neale, and P. J. Rasch, 2009: An evaluation of ENSO asymmetry in the Community Climate System Models: A view from the subsurface. *J. Climate*, **22**, 5933–5961.
- Zhang, Y., J. M. Wallace, and D. S. Battisti, 1997: ENSO-like interdecadal variability: 1900–93. *J. Climate*, **10**, 1004–1020.